Toronto Metropolitan University

Department of Aerospace Engineering
Faculty of Engineering & Architectural Science

Course Number	AER 821
Course Title	Space Attitude Dynamics
Semester/Year	Fall 2025
Instructor	John Enright

Lab Report No.	4

Report Title	Lab 4 Report

Section No.	02
Submission Date	6th, November, 2025
Due Date	6th, November, 2025

Name	Student ID	Signature*
Aidan Walpole	XXXX07770	A.W.
Bosco Mak	XXXX04446	
Stefan Aquino	XXXX92196	

(Note: remove the first 4 digits from your student ID)

**By signing above, you attest that you have contributed to this submission and confirm that all work you have contributed to this submission is your own work. Any suspicion of copying or plagiarism in this work will result in an investigation of Academic Misconduct and may result in a "0" on the work, an "F" in the course, or possibly more severe penalties, as well as a Disciplinary Notice on your academic record under the Student Code of Academic Conduct, which can be found online at:http://www.ryerson.ca/senate/policies/pol60.pdf.*

Table of Contents

Table of Equations

1. Introduction

Reaction wheels are one of the most common actuators used for spacecraft attitude control, providing accurate orientation changes without the use of propellant. They operate on the principle of angular momentum exchange; when a motor accelerates a flywheel, the spacecraft experiences an equal and opposite torque. Being able to adjust pointing using internal torques makes reaction wheels ideal for long missions that require fine stability and low-disturbance maneuvers.

In this experiment, a reaction wheel system consisting of a DC motor and an aluminum flywheel mounted on a load cell was used to study the relationship between electrical input and mechanical response. The system was controlled through a MATLAB Simulink interface that allowed the user to apply step and ramp voltage commands, record sensor data, and evaluate the motor's torque output and behaviour.

The objective of this lab is to model and test the torque generation of the reaction wheel under both open-loop and closed-loop conditions. In the open-loop condition, voltage ramp rates are used to control the current through the motor, and with the known motor resistance and torque constant, determine the resulting torque. In the closed-loop condition, two feedback controllers are developed and tested: an integral current controller that regulates torque through current control, and a nested PID velocity controller that maintains torque by controlling wheel speed. These results are compared to theoretical predictions to evaluate the accuracy, performance, and the effects of friction, vibration, and other non-ideal factors.

2. Theory

A reaction wheel system controls a spacecraft's orientation by turning electrical energy into angular momentum. According to Newton's third law, every action creates an equal and opposite reaction. When the motor speeds up or slows down the flywheel, it applies an opposite torque to the spacecraft, allowing it to rotate about its axes without firing thrusters or using fuel.

Table 2.1 summarizes the variables we will discuss below. All values were obtained directly from the lab manual:

Table 2.1: *Wheel and Motor Parameters*

Parameter	Symbol	Value
Motor Resistance	R	0.83 Ω
Torque/Current Constant	K	0.0182 Nm/A
Moment of Inertia (Motor)	J□	4.17×10^{-6} kg·m²
Inductance	L	0.63×10^{-3} H
Wheel Friction	D	2.61×10^{-6} Nm/(rad/s)
Wheel Mass	m_x	0.324 kg
Wheel Moment of Inertia	Jw	9.4161×10^{-4} kg·m²
Current	I	A
Voltage	E	V
Torque	M	Nm
Motor Speed	$\dot{\theta}$	rad/s

During the lab, the reaction wheel is driven by a DC motor, where the torque generation is directly proportional to the motor's current. The relationship is expressed as:

$$M = KI$$

Eq (1): *Motor Torque-Current Relationship*

Where M is the torque produced by the motor (Nm), K is the motor torque constant (Nm/A), and I is the current (A). The motor's electrical dynamics are governed by the following equation:

$$E = RI + L\frac{dI}{dt} + K\frac{d\theta}{dt}$$

Eq (2): *Ohm's Law with EMF*

Where E is the applied voltage (V), R is the motor resistance (Ω), L is the inductance (H), and $K\frac{d\theta}{dt}$ represents the back electromotive force (EMF) generated by the spinning motor.

The mechanical response of the system can be described by Newton's second law for rotation:

$$M = J\frac{d^2\theta}{dt^2} + D\frac{d\theta}{dt}$$

Eq (3): *Rotational Dynamics of the System*

Where J is the combined moment of inertia of the wheel and motor, $\frac{d\theta}{dt}$ is the angular velocity (rad/s), and D is the damping coefficient (Nm·s/rad). The first term represents the torque required to accelerate the wheel, while the second term accounts for energy losses due to forces like friction and drag.

Table 2.2 contains the operating envelope for the reaction wheel. All values were obtained directly from the lab manual:

Table 2.2: *Reaction Wheel Operating Envelope*

Parameter	Value
Max. Motor Voltage	9.4 V
Max. Voltage Step	4.0 V
Max. Current	± 3 A
Max. Load Cell Torque	0.1 Nm
Wheel Speed	$200 \leq \dot{\theta} \leq 500$ rad/s

Combining the electrical and mechanical models allows the system to be represented as a transfer function relating input voltage to angular velocity. For this system, the transfer function from voltage E to wheel speed $\frac{d\theta}{dt}$ is:

$$\frac{\frac{d\theta(s)}{dt}}{E(s)} = \frac{K/(JL)}{s^2 + (\frac{D}{J} + \frac{R}{L})s + \frac{DR + K^2}{JL}}$$

Eq (4): *Voltage-to-Speed Transfer Function*

This relationship shows how the input voltage influences the resulting rotational motion. Similarly, the voltage-to-torque transfer function can be written as:

$$\frac{M(s)}{E(s)} = \frac{K/L(s + KD/(JL))}{s^2 + (\frac{D}{J} + \frac{R}{L})s + \frac{DR + K^2}{JL}}$$

Eq (5): *Voltage-to-Torque Transfer Function*

This shows that torque depends on both the electrical and mechanical properties of the reaction wheel assembly.

During testing, in open-loop operation, the motor torque can be estimated from the input voltage using the known resistance and torque constant, while effects like inductance and damping are small enough to be neglected. When switched to closed-loop operation, feedback is introduced to make the system more stable and accurate. The current controller keeps the torque constant by holding the current steady, while the PID velocity controller changes the motor voltage to reach the target angular acceleration.

3. Procedure

3.1 Open-Loop Reaction Wheel Control Procedure

1. The reaction wheel hardware was powered ON, and the GUI was opened.
2. Several preliminary step tests were run through the GUI to ensure proper system operation.
3. The test data was exported and reviewed in Excel to confirm that everything was recorded correctly.
4. The voltage ramp rates, calculated in *Pre-Lab 1,* were used to perform the open-loop ramp tests.
    - Two ramp tests were run, with data collected for each case.
    - Plots were used to compare the commanded torque, measured torque, and torque estimate from the current for both high-torque and low-torque tests.
    - The accuracy of each torque estimate was discussed, and differences between the high and low torque results were analyzed.
5. Four additional ramp rate tests were performed.
    - The steady-state torque for each test was calculated.
    - The shape of the curve was compared to our results from *Pre-Lab 1*.
6. The *AER821_Lab3_RW_Part_D_E.mdl* Simulink file was opened.
7. An open-loop ramp input to the motors was generated (identical to the 5×10^{-3} Nm input)
8. The sensor output was recorded with similar results to those obtained previously.

3.2 Closed-Loop Reaction Wheel Control Procedure

1. An integral (*I*-type) controller for current was implemented.
2. Plots were generated to show the torque profiles for steps of $\pm\ 5 \times 10^{-3}$ Nm and $\pm\ 10 \times 10^{-3}$ Nm, showing the actual and theoretical current, and the actual (from load cell) and theoretical (from current) torque.
3. The velocity controller performance was tuned and evaluated based on appropriate performance metrics.
4. The above torque tests were repeated.
5. The performance of the two controllers (integral and velocity) was compared.
6. Two simple constant torque maneuvers were generated (identical except for the initial wheel speed).
    - The first passes through zero wheel speed.
    - The second always has an initial bias value.

4. Results

4.1 Pre-Lab 1

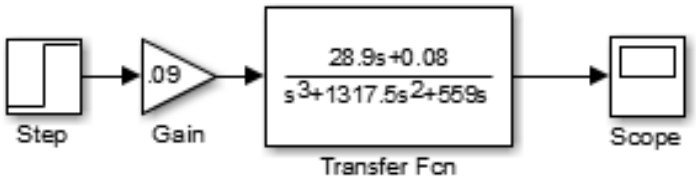

Figure 4.1.1: *Open-loop Simulink Model (0.09 V/s)*

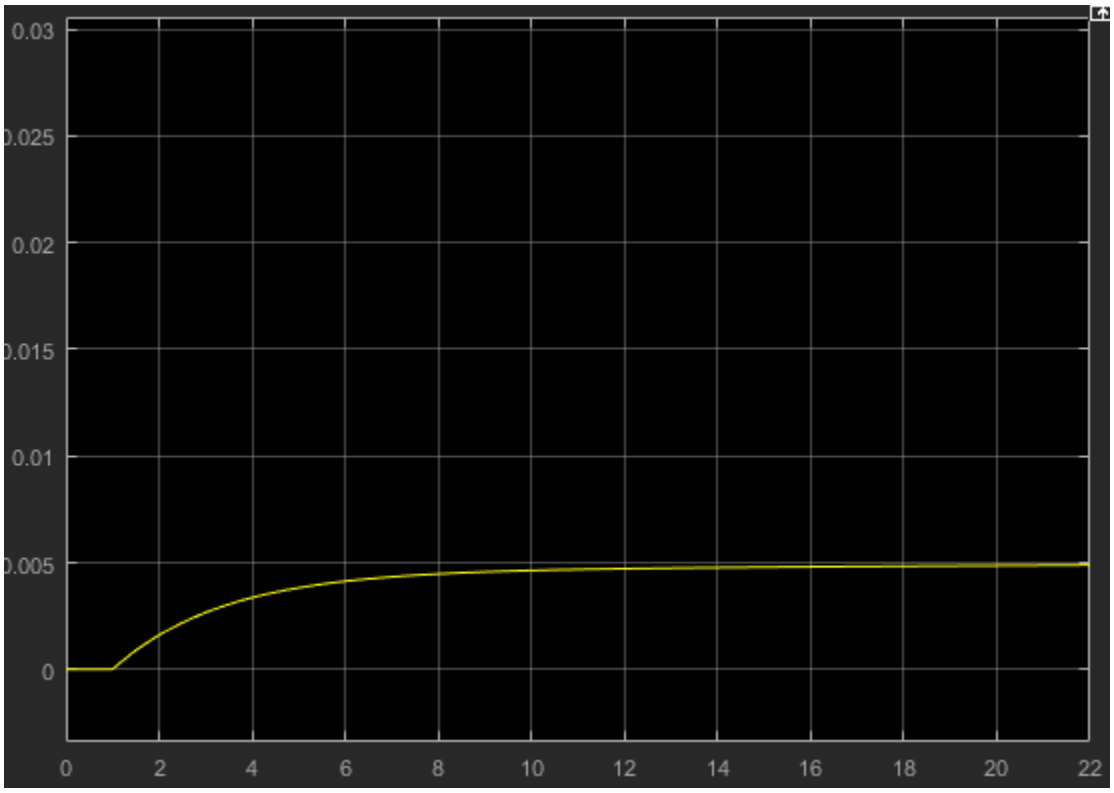

Figure 4.1.2: *Torque (Nm) at Voltage Ramp Rate of 0.09 V/s*

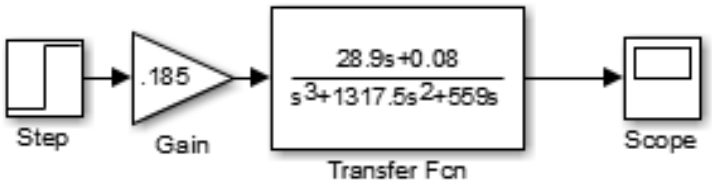

Figure 4.1.3: *Open-loop Simulink Model (0.185 V/s)*

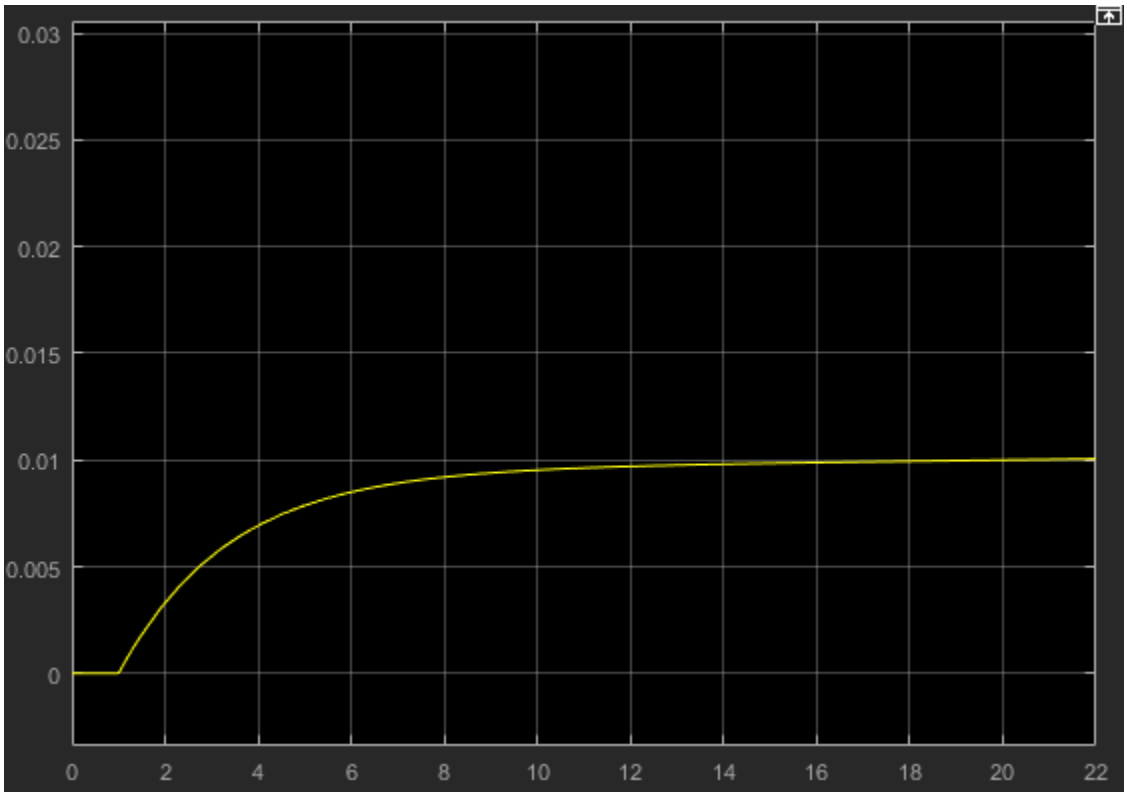

Figure 4.1.4: *Torque (Nm) at Voltage Ramp Rate of 0.185 V/s*

Table 4.1.1: Simulated Values of the Voltage Ramp Rate

Voltage Ramp Rate (V/s)	Torque (Nm)
0.09	~0.005
0.185	~0.01

4.2 Pre-Lab 2

The prelab asked for three different Simulink models: one with a PID controller, one with just an integral controller, and the third with a nested velocity controller. Each was designed using the listed values from *Tables 4.2.1* and 4.*2.2*, specifically *J*, *D*, and the voltage and speed envelopes.

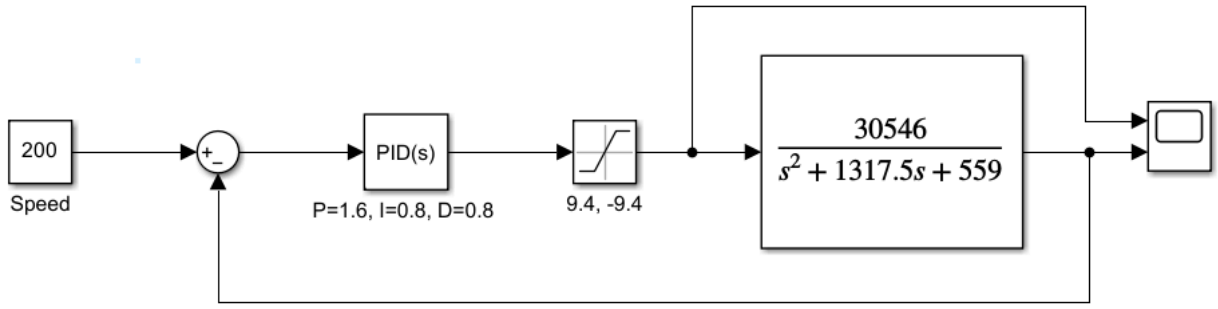

Figure 4.2.1: *Simulink Model for the PID Controller*

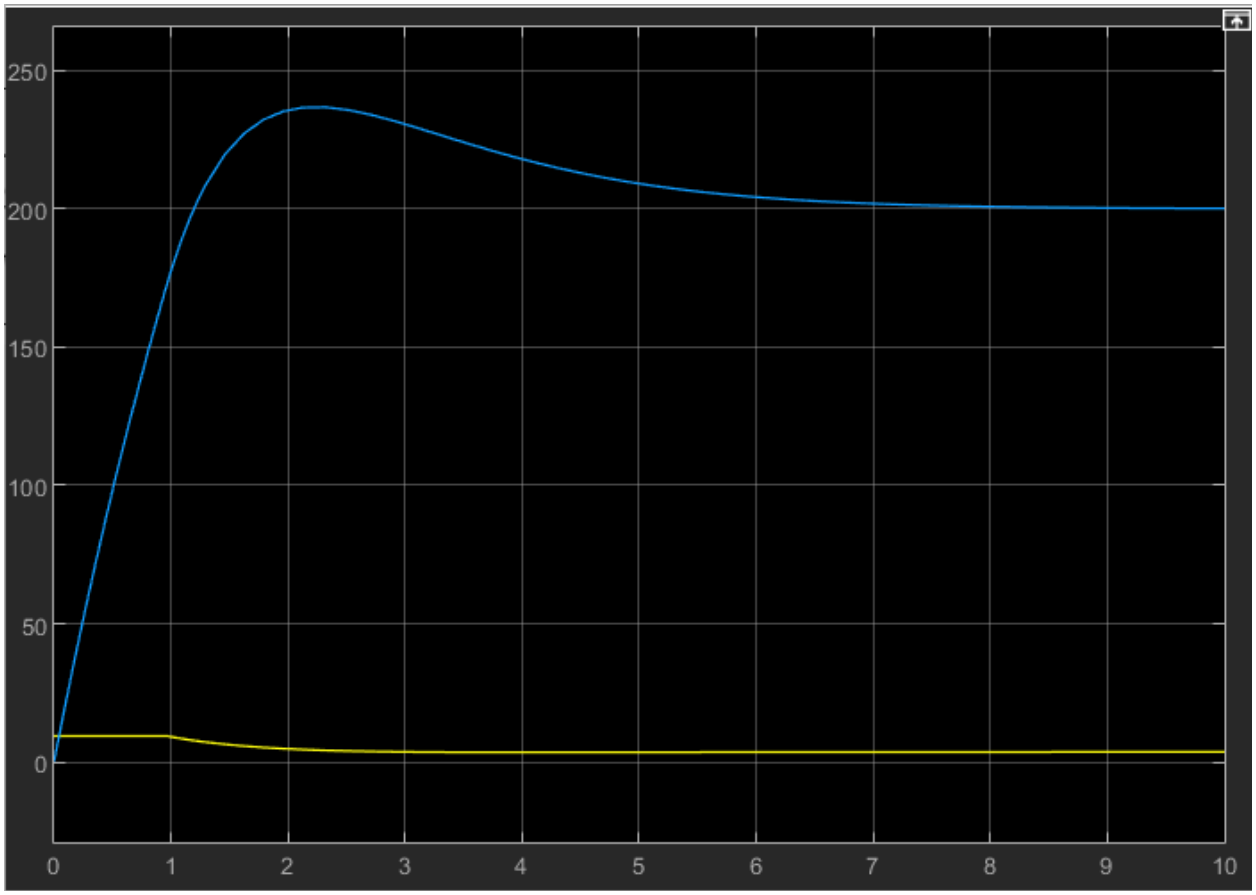

Figure 4.2.2: *Simulink Output for the PID Controller*

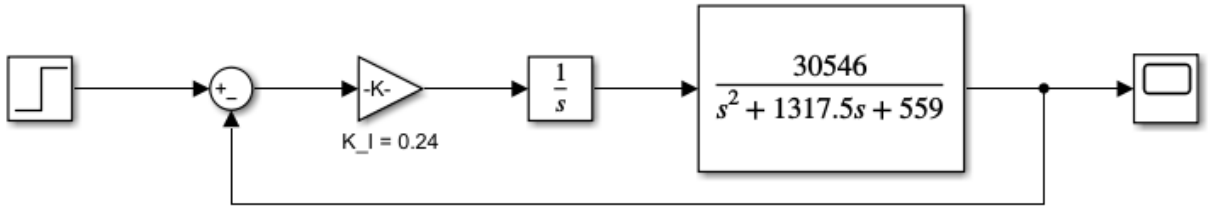

Figure 4.2.3: *Simulink Model for the Integral Controller*

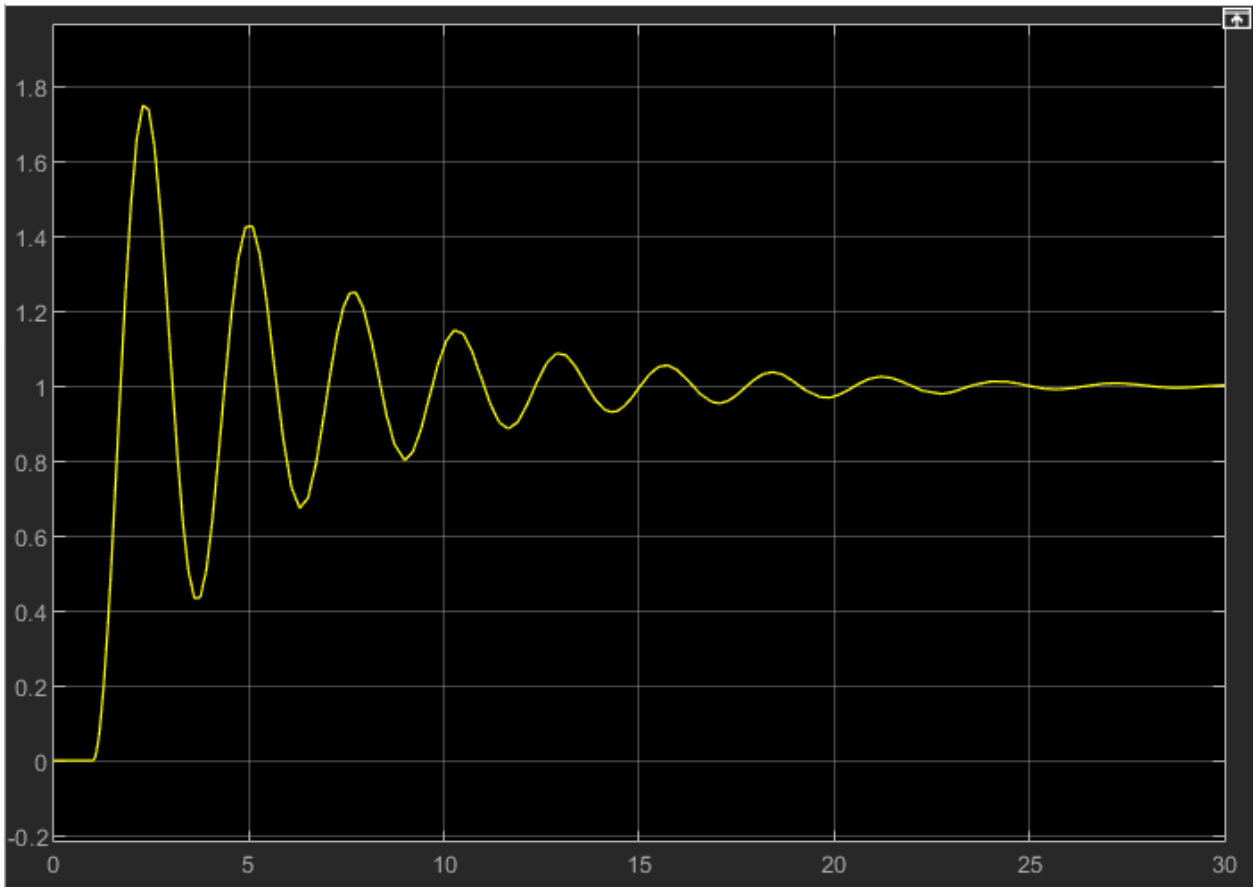

Figure 4.2.4: *Simulink Output for the Integral Controller*

The PID and integral controllers both created a closed-loop feedback system to allow for live response to current conditions, such as speed, voltage, and disturbances. The PID model is much more advanced than the integral model, as it includes the same integrator term, along with proportional and derivative controls as well. This causes it to settle in a fraction of the time compared to the integral controller. The PID controller also includes a 9.4, -9.4 V envelope to prevent the simulation from applying excessive voltage to the hardware.

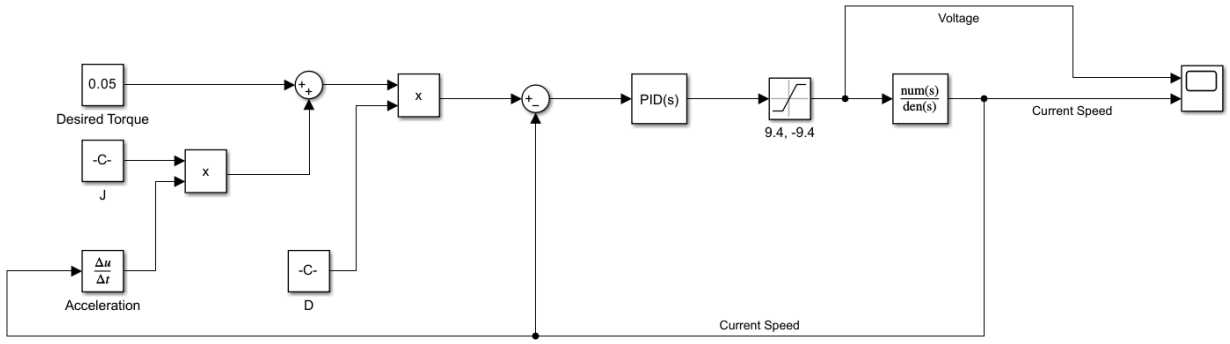

Figure 4.2.5: *Simulink Model for the Nested Velocity Controller*

The nested velocity controller builds upon the first model (the PID controller), making use of *Equation (3), Rotational Dynamics of the System*, to control the model's angular velocity through a desired torque input:

$$M = J\frac{d^2\theta}{dt^2} + D\frac{d\theta}{dt}$$

Rearranging:

$$\frac{d\theta}{dt} = \frac{M - J\frac{d^2\theta}{dt^2}}{D}$$

Thus, with a desired torque, wheel inertia, and friction constant values, the corresponding angular velocity can be calculated. This will be fed back into the original PID controller and used on the reaction wheel.

4.3 Open-Loop Reaction Wheel Control

The ramp test was run for expected torque values of 0.005 and 0.01 N/m with voltage ramp rates of 0.1 and 0.185 v/s, respectively. The resulting plots of the generated torque and the calculated estimates from speed and current values can be found below in *Figures 1 & 2*.

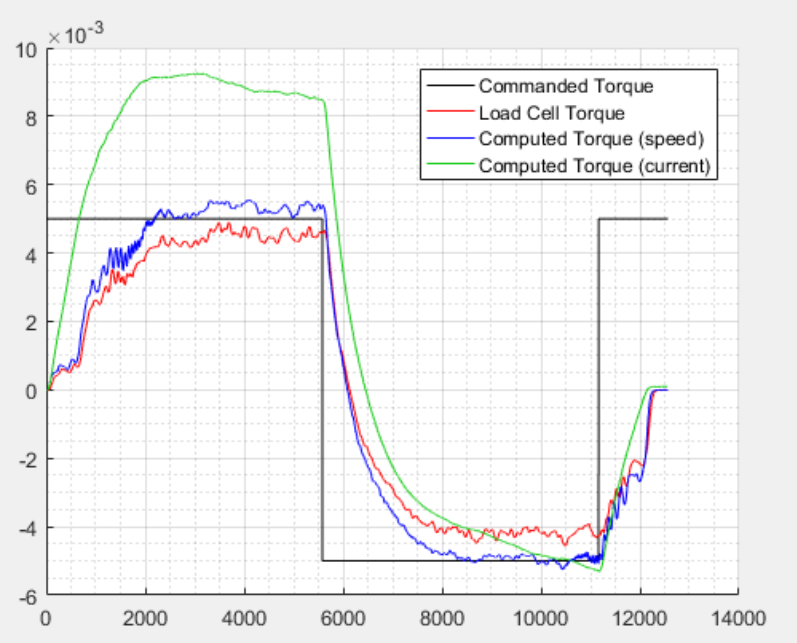

Figure 4.3.1: *Torque Comparison Graph for Voltage Rate of 0.100 V/s*

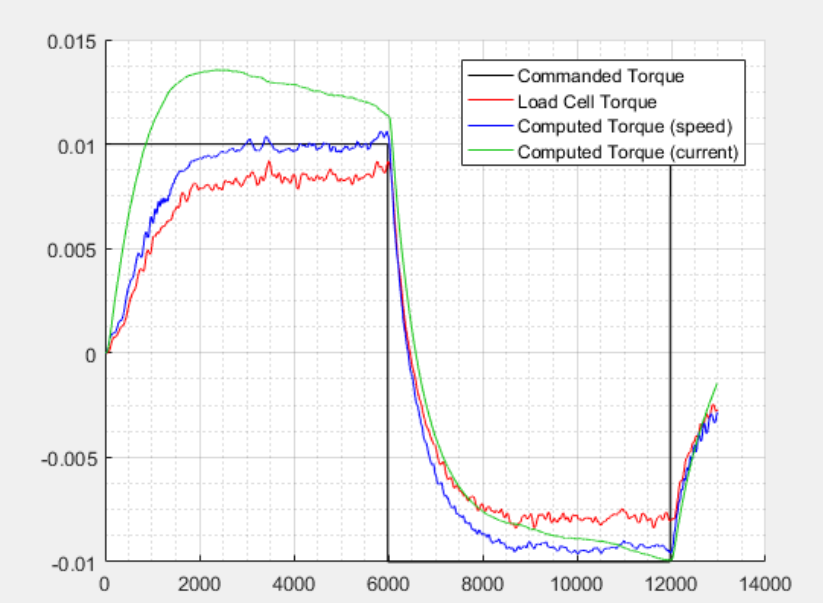

Figure 4.3.2: *Torque Comparison Graph for Voltage Rate of 0.185 V/s*

Within the figures, the commanded torque created the expected step function in both tests, with values of 0.005 and 0.01 altering polarity. The measured torque from the load cell represents the real torque, represented by the red line. Its curve follows the expected trend of the commanded torque but is consistently lower than expected, indicating losses through damping and friction. In the higher torque chart, this error between command torque and experimental torque is larger, revealing….

The computed torques from the angular speed are represented by the blue line, and follow a similar trend to the measured torque, but show much better performance, with less error between the expected and calculated torques, suggesting that this theoretical model aligns well with both the real-world behaviour and expected outcome. The torque calculated through current, represented by the green line, displays a large overshoot and large steady state error. This discrepancy is likely due to the fact that the reading comes straight from the electrical source, so it does not consider any effects from the motor, which the speed calculations would, due to the fact that speed readings come directly from the motor.

Overall, these plots reveal that while current can be used to estimate the expected torque, dynamic estimation from speed data provides more accurate values if direct measurement is not available. Completing the ramp test on expected torque values of 0.0075, 0.0125, 0.015, and 0.02 yields *Figures 3-6*.

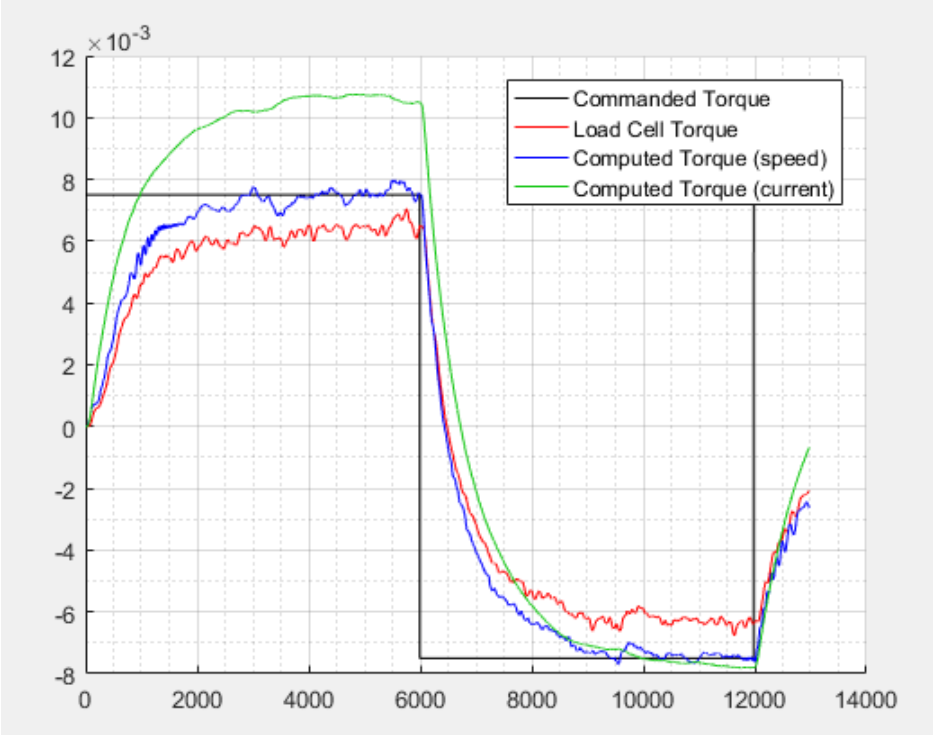

Figure 4.3.3: *Torque Comparison Graph for Voltage Rate of 0.145 V/s*

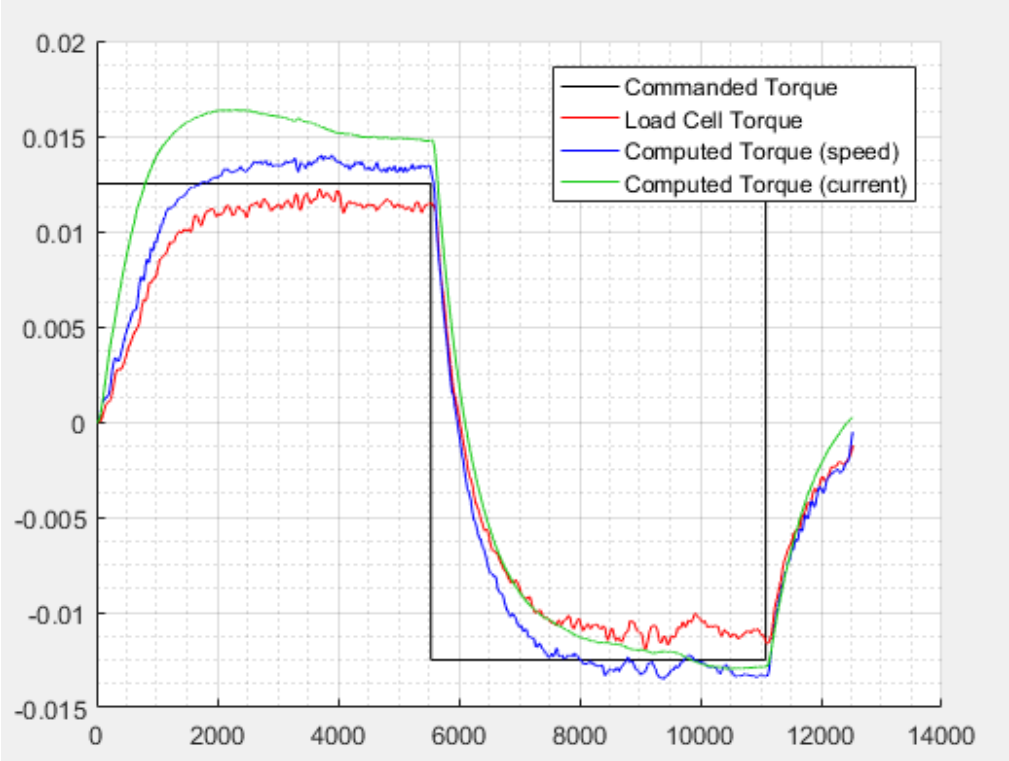

Figure 4.3.4: *Torque Comparison Graph for Voltage Rate of 0.225 V/s*

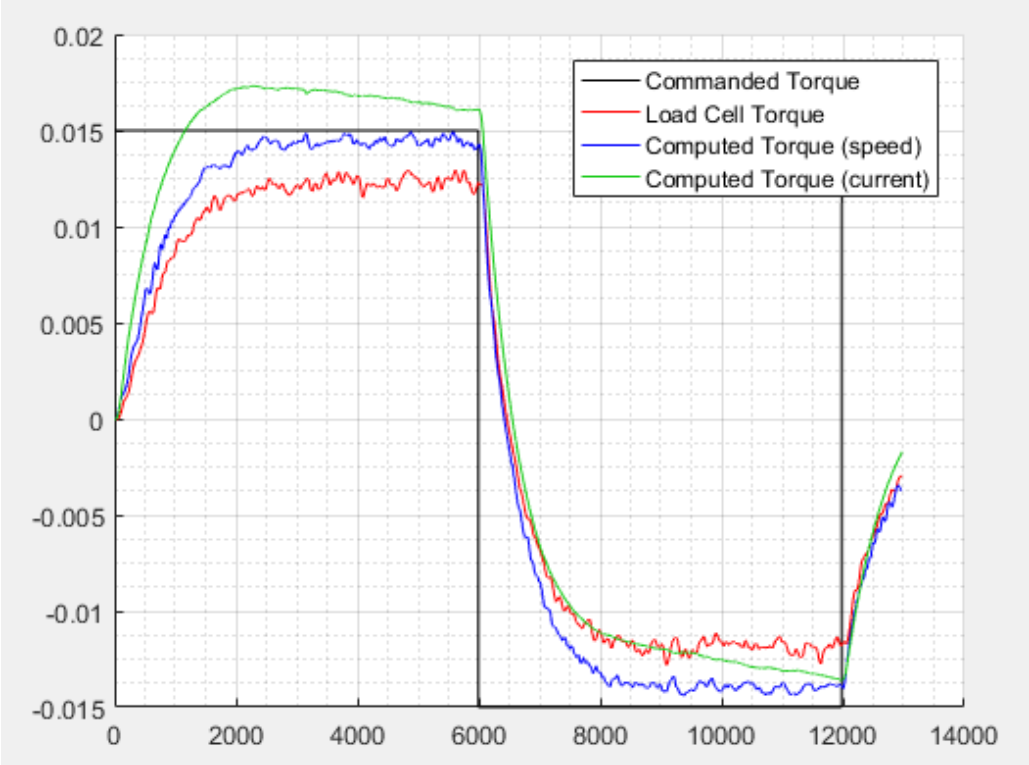

Figure 4.3.5: *Torque Comparison Graph for Voltage Rate of 0.275 V/s*

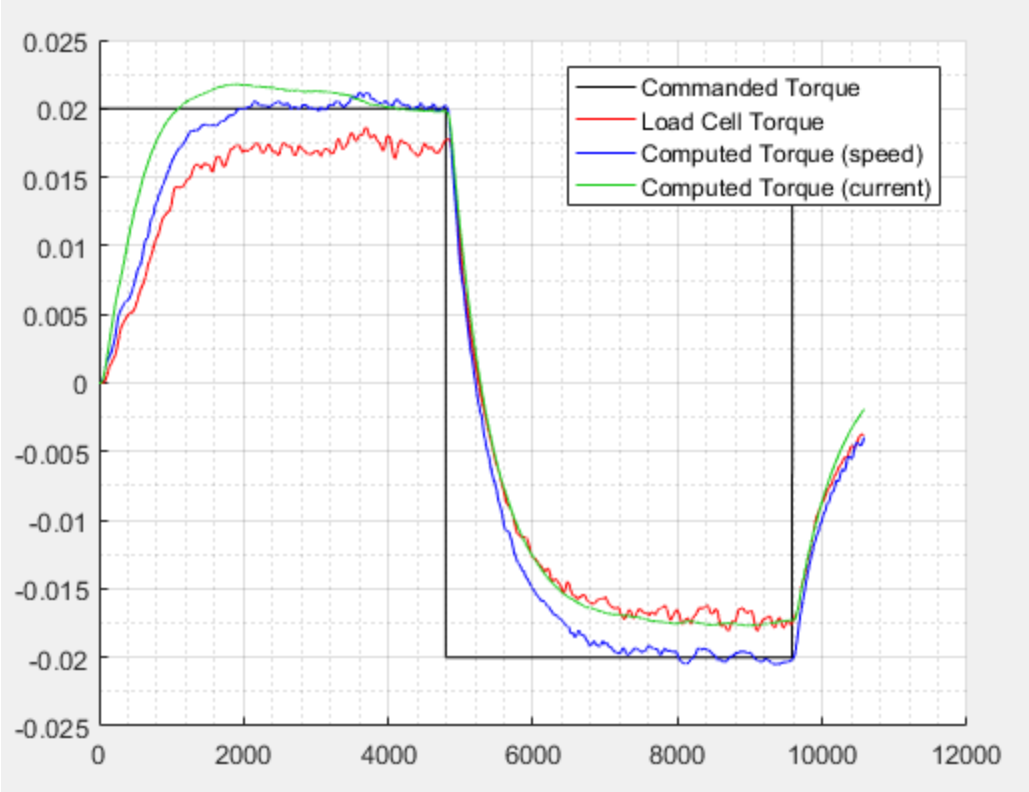

Figure 4.3.6: *Torque Comparison Graph for Voltage Rate of 0.385 V/s*

The average steady state torque values will be extracted from these figures by taking the average reading from the load cell torque values (red line). These values, along with the expected torque and the related voltage rate, are tabulated in *Table 3.1*.

Table 4.3.1: *Expected Torque Values vs Average Steady State Torque*

Expected Torque	Voltage Rate	Steady State Torque
0.0050	0.100	0.0045
0.0075	0.145	0.0060
0.0010	0.185	0.0085
0.0125	0.225	0.0110
0.0150	0.275	0.0120
0.0200	0.385	0.0175

Plotting these torque values vs the voltage rate will visualize the difference between the theoretical torque values determined in the pre-lab and the experimental values. See *Figure 7*.

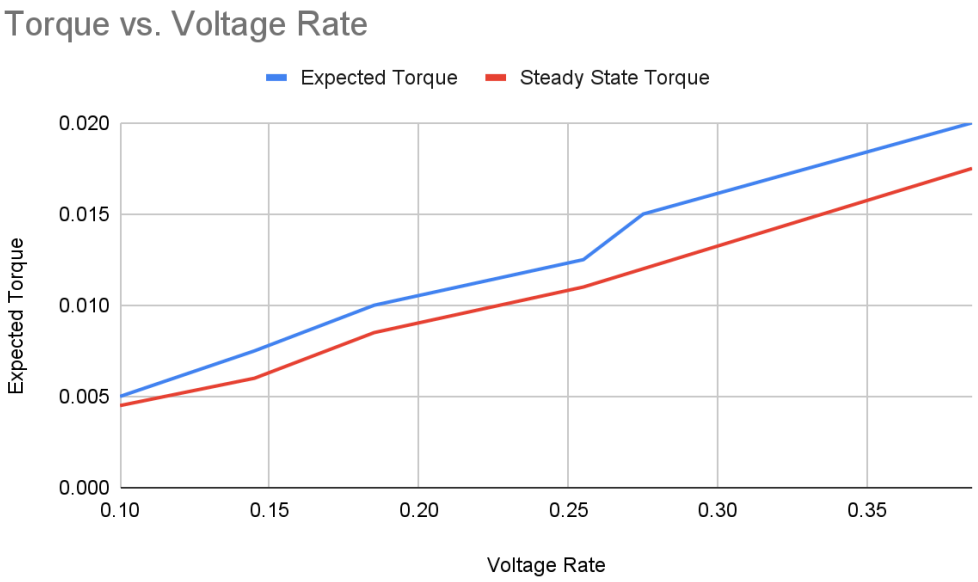

Figure 4.3.7: *Expected Torque vs. Voltage Rate*

The expected torque is represented by the blue line and is the plot of the theoretical values of torque plotted against the voltage rates calculated by the Simulink model. The red line represents the measured torque plotted against the same voltage rates that were input into the ramp test. Both curves follow the same linear trend; however, the experimental values remain consistently below the theoretical curve, indicating the same losses due to friction and damping mentioned previously. Furthermore, the difference between the two curves seems to grow as the voltage rate increases, suggesting these effects grow with voltage rate. Overall, these figures confirm the proportional relationship between voltage rate and torque predicted in the pre-lab, while highlighting the discrepancies caused by real-world systems and non-ideal dynamics.

4.4 Closed-Loop Reaction Wheel Control

The integral controller simulation had a few strange discrepancies, but otherwise simulated and experimental results were similar. Figure 4.4.1 shows the current plots of the integral controller, showing commanded, measured, and calculated values. During lab set-up, the polarity of the input was swapped, resulting in the commanded and actual current values to swap signs. However, the magnitude of the values remain relatively consistent. There is a slight negative bias in the load cell current, which prevented the current from settling at the desired current in the positive polarity and causes a large settling time in the negative polarity.

The bias in the current may be explained by the voltage plot. Figure 4.4.2 shows the voltage applied through the simulation. Sudden spikes in voltage align with impulses seen in the current and torque graphs. A large spike occurs at the beginning of the simulation to overcome the wheel's inertia, with subsequent spikes in voltage a result of error rather than feature, potentially from system vibrations.

Furthermore, the voltage readings themself are positively biased. The simulations should apply +/-1 V and +/- 2V in the 5 and 10 microNewton-meter simulations respectively. The voltages never settle at the negative end range, prevalent in the 10 mNm simulation.

The measured torque never settled at the commanded torque output. Figure 4.4.3 shows the torque seems to under-settle half the magnitude with positive-commanded torques, but responds better to negative applied torque. This error may be a result of the overall commanded torque being very small, only on the scale of microNewton-meters. Response seems to more accurately resemble commanded torque with higher values, as seen with the 10 mNm simulation.

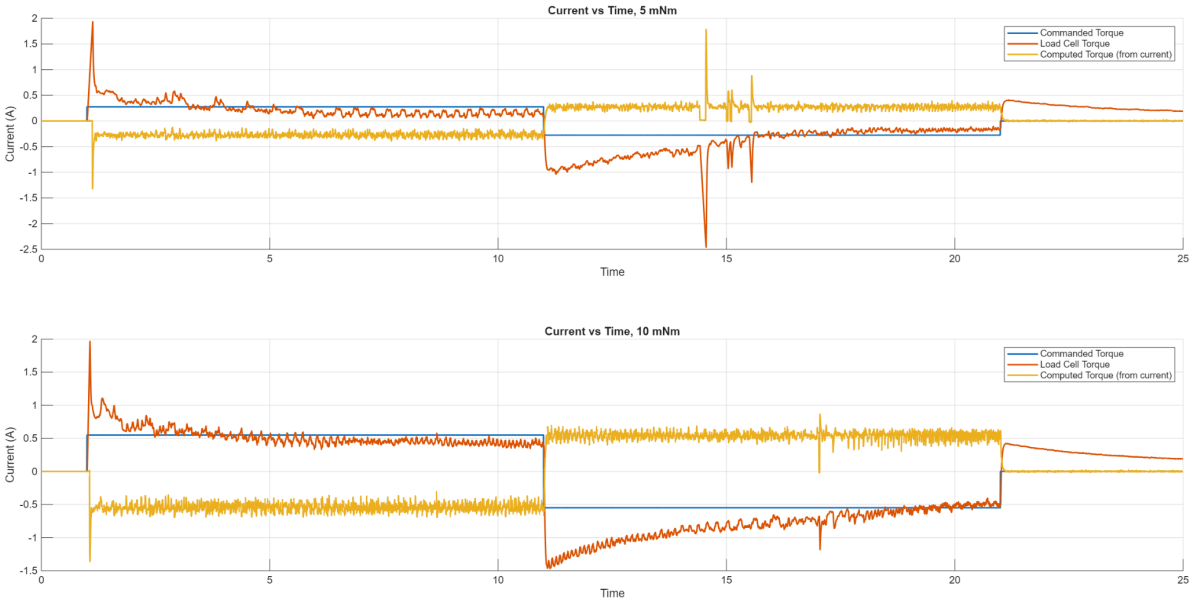

Figure 4.4.1: *Integral controller plots, current.*

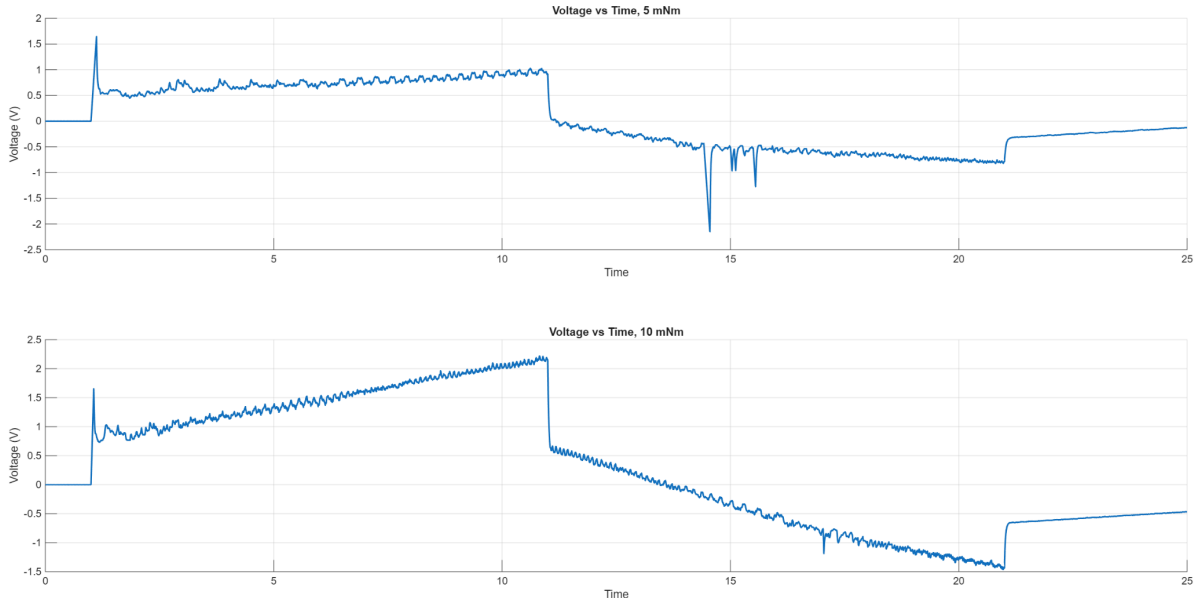

Figure 4.4.2: *Integral controller plots, voltage.*

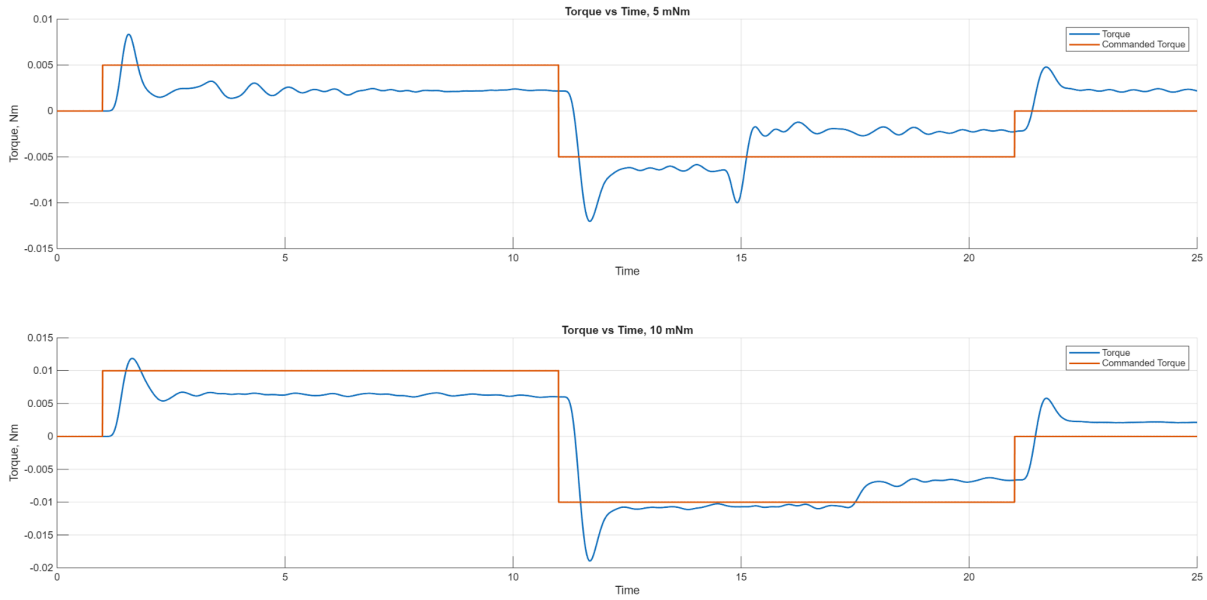

Figure 4.4.3: *Integral controller plots, torque.*

The PID speed controller provides a much more accurate simulation of the torque, likely since wheel speed is affected by the same losses as the torque. Since the integral controller only simulated values based on direct electrical inputs, it could not account for losses such as friction and damping. Conversely, simulating based on wheel speed better accounts for these losses as wheel speed is dependent on electrical input.

Figure 4.4.4 shows the RPM of the wheel throughout the simulation. The computed RPM is nearly the same as the commanded RPM, varying only slightly in the beginning where a large voltage output is necessary to overcome the wheel's inertia. The wheel speed is notably higher than

commanded and calculated values as it increases, likely due to requiring more angular velocity to account for energy losses in friction and damping. Once the wheel's speed peaks and begins to decrease, these losses do not need to be overcome and are less noticeable, resulting in closer values to calculated and commanded values. However, the effect of these losses are more noticeable at higher speeds, as shown in the second simulation of 10 microNewton-meters where the measured RPM drops faster than the calculated and commanded values.

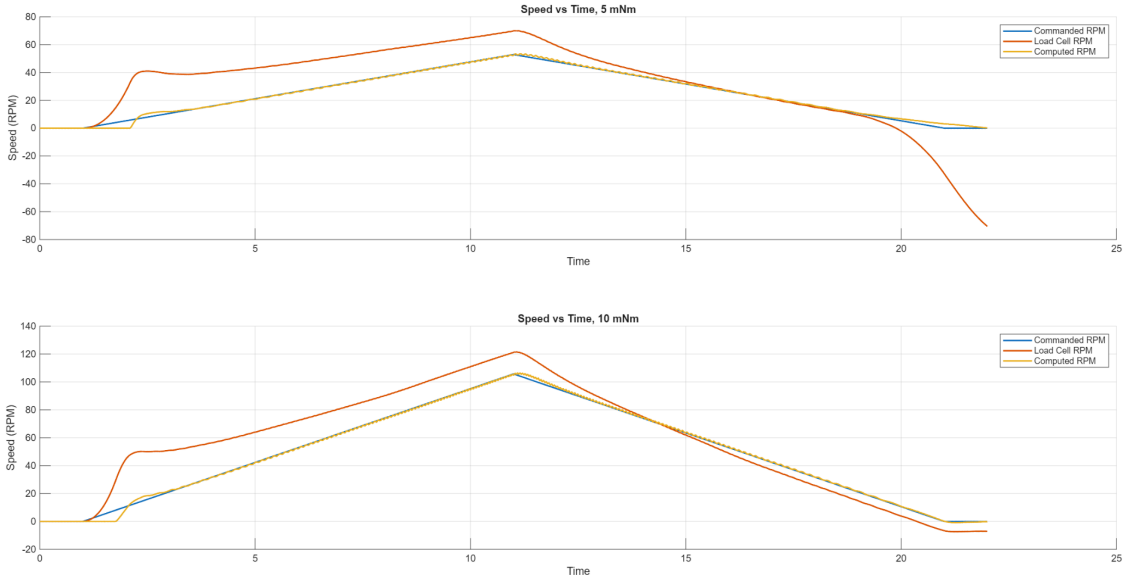

Figure 4.4.4: *Velocity controller plots, RPM.*

Figure 4.4.5 shows the voltage through the simulation. A large voltage spike occurs at the beginning to overcome the wheel's inertia. Voltage noise increases as the wheel continues to accelerate, which may produce vibrations affecting the cables connected to the wheels. This hypothesis is in line with the graphs as noise is most dense at peak speeds, which is also observed in the integral controller to a lesser degree. Both voltage graphs also show a dip below zero, which is more pronounced in the 5 mNm experiment. This may be due to the system aiming to decelerate the wheel faster, resulting in some overshoot.

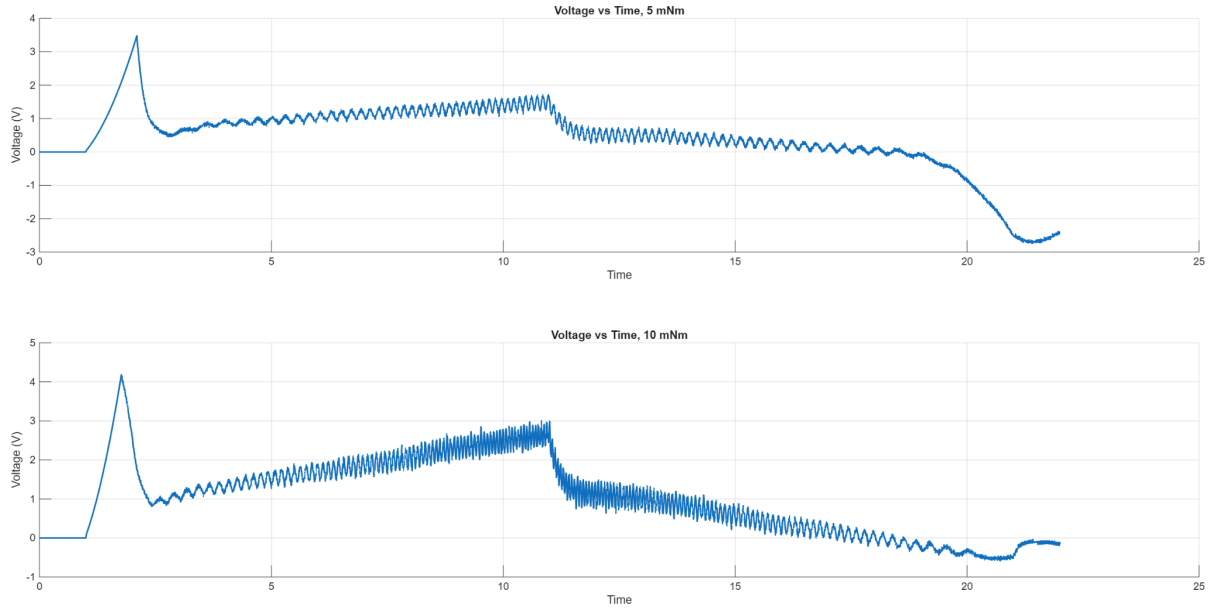

Figure 4.4.5: *Velocity controller plots, voltage.*

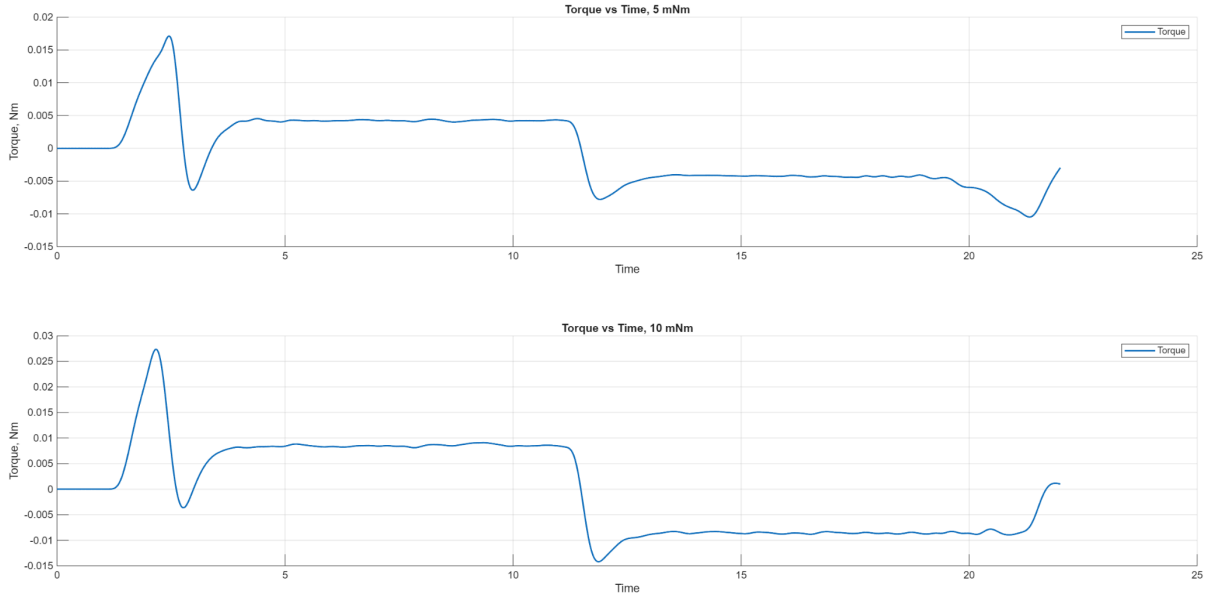

Figure 4.4.6: *Velocity controller plots, torque.*

Figure 4.4.6 shows the torque from the simulation. Disregarding the initial voltage input required to overcome inertia, the overshoot of the system is about 50%, settling at values just below the expected. This plot shows that the speed controller is much more precise than the current controller in its ability to command torque, with much less steady state error and overshoot.

As seen in both the current and speed controllers, higher commanded torques are easier to simulate and measured values are much closer to the expected. This is due to overcoming static friction, which is much more pronounced at low-magnitude experiments such as this. Operating on the scale of microNewton-meters seems to operate within the threshold of motion, which may explain some high initial overshoot values. The expected initial force required to start the system may be too

low to overcome static friction, and energy losses may occur along the signal path. The system adjusts its output based on the error feedback and continues to increase its output. At the point where the system begins to move, it rapidly accelerates and feedback is too slow to respond to it, resulting in high initial overshoot.

Kinetic friction effects diminish at higher speeds and greater torques, but other losses such as damping and vibrations take over. Furthermore, the second half of all experiments (when voltage is negative) provides more accurate values than their initial counterparts, achieving a lower overshoot and steady state error. The effects of static friction do not apply to the wheel at the direction change since the wheel is already spinning, and therefore does not need to overcome it or its own inertia.

To clearly determine the effects of static friction, two torque maneuvers were performed. Figure 4.4.7 demonstrates this experiment in which initial conditions for torque response vary, with a torque of 5 mNm applied at 10 seconds. The top plot shows the torque response with an initial positive wheel bias, showing a low overshoot, fast settling time, and low steady state error. The bottom plot shows the torque response starting from zero, which shows a high overshoot and longer settling time, eventually reaching a similar steady state error. These torque maneuvers echo results from the previous experiments and follow the same trend of a high initial overshoot. This reinforces the idea that inertia and static friction must be overcome before the system becomes stable. This is prevalent even in the initial bias torque maneuver, where a torque of 1.5 mNm is commanded but the system overshoots by nearly 100% before settling.

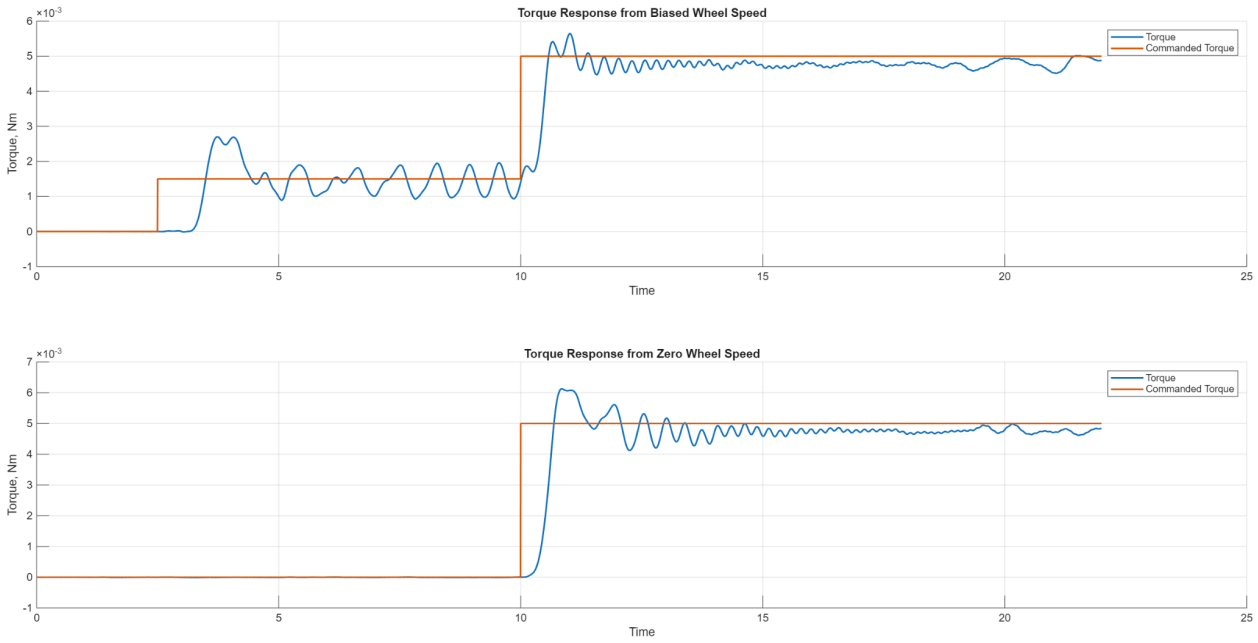

Figure 4.4.7: *Torque maneuvers with biased vs zeroed wheel speed.*

5. Conclusion

This lab demonstrated the relationship between electrical input and reaction wheel dynamics, specifically torque and angular velocity. Feedback control was proven to be a crucial component to improving torque accuracy. In the open-loop tests, the torque increased proportionally to the applied voltage ramp rate, aligning with theoretical predictions. Measured torque was consistently below expected values, a reflection of energy losses from friction, damping, and structural vibrations. The torque calculated from angular velocity measurements aligned much more closely with measured values than torque calculated from current, showing that dynamic feedback from the wheel's motion captures nuances which electrical estimates cannot.

In the closed-loop portion, the integral current controller successfully commanded torque direction and general magnitude, but exhibited slow settling, steady-state error, and strong sensitivity to biases and disturbances. In contrast, the nested velocity controller provided faster convergence, reduced steady-state error, and a closer match to theoretical torque profiles. Since the controller measures the wheel directly rather than raw electrical input, it includes any energy losses along the path to the wheel including friction and damping, leading to more accurate torque control. However, both controllers demonstrated performance limitations at very low commanded torques, where losses are relatively large compared to the desired output due to static friction. The effect of static friction and the overcoming of inertia were tested using two torque maneuvers using different initial conditions, which determined an initially moving wheel will have a better torque response than its still counterpart.

Overall, this lab confirmed the theoretical torque–current relationship and the proportional effect of voltage ramp rate, while clearly illustrating the limits of open-loop control for precision attitude actuation. Closed-loop simulations, particularly those using velocity feedback, significantly improve system performance by inherently accounting for energy losses. These findings emphasize why spacecraft attitude control systems rely on feedback-driven reaction wheel control rather than purely feedforward torque commands, especially in missions requiring fine pointing accuracy and long-duration stability.